J|A|C|S
ARTICLES
Published on Web 09/25/2002

Molecular Dynamics Simulation Study of the Negative Correlation in Antibody AZ28-Catalyzed Oxy-Cope Rearrangement

Toshio Asada,*,† Hiroaki Gouda, and Peter A. Kollman‡

Contribution from the Department of Pharmaceutical Chemistry, University of California, San Francisco, California 94143-0446

Received June 3, 2002

Abstract: The oxy-Cope rearrangement reaction in the antibody AZ28 is investigated using ab initio molecular orbital calculations and molecular mechanical molecular dynamics simulations. This antibody, AZ28, is known as one of the few systems where the mature catalytic antibody shows a negative correlation between the transition state analogue (TSA) binding affinity and the catalytic rate of the oxy-Cope rearrangement compared to the germ line catalytic antibody. The ab initio optimized structure shows that the transition state structure has a more planar configuration than the TSA. The favorable electrostatic interactions between AZ28 and the transition state analogue overcome the unfavorable van der Waals interactions; thus, AZ28 shows higher binding affinity for the TSA than the germ line. However, the AZ28 is not flexible enough to accept the relatively planar transition state structure. Because the lower flexibility causes poorer antibody−hapten interaction energies, the activation free energy of the oxy-Cope rearrangement becomes larger in the mature antibody than the germ line. We show that the differences in flexibility between the germ line and the mature form and the differences in structure between TSA and the transition state are the origin of the negative correlation in AZ28-catalyzed oxy-Cope rearrangement. The mutation of residue 34 of the light chain, 34^L, affects the binding free energies through the interresidue interaction because it is the closest to the hapten among the six mutatable residues. However, it does not affect the negative correlation.

Introduction

The immune response system produces high-affinity antibodies to protect the host from disease. At the first stage, the germ line antibody is created by forming the functional antibody gene from the V, D, and J gene segments. After generating the germ line antibody, the immune response system introduces point mutations[1] in the germ line to create the mature form with high affinity for the hapten. In general, experiments have been carried out by generating the corresponding antibody for a given hapten. These antibody−hapten complexes provide good opportunities to characterize the structural basis of affinity maturation and mutational effects on the catalytic rate of the antibody. For these purposes, many kinds of antibodies[1−3] are elicited by the different kinds of hapten.

Recently, the antibody AZ28 was generated[4,5] to the transition state analogue (TSA) of the oxy-Cope rearrangement[6−9] which is an unusual pericyclic reaction that is widely used in organic synthesis. This rearrangement could occur by two different diradical pathways[6,8] and is not catalyzed by any known enzyme.[4,5] Interestingly, this antibody−hapten complex is one of the few systems where a negative correlation is observed between TSA binding affinity and the catalytic rate of the oxy-Cope rearrangement. This antibody AZ28 catalyzes the oxy-Cope rearrangement with $k_{cat}/k_{uncat} = 5300$, a K_M of 74 μM, and K_D of 17 nM. As is expected, the germ line antibody has a lower binding affinity for TSA ($K_D = 670$ nM) than AZ28 but, surprisingly, a higher catalytic rate, $k_{cat}/k_{uncat} = 163\,000$, a K_M of 73 μM.[5]

In this contribution, we study this negative correlation in the AZ28−hapten complex by using molecular dynamics (MD) simulations[10] and the molecular mechanics-Poisson Boltzmann/surface area (MM-PB/SA) method developed by Srinivasan et

* To whom correspondence should be addressed. E-mail: asada@ms.cias.osakafu-u.ac.jp.

† Current Address: Department of Chemistry, College of Integrated Arts and Sciences, Osaka Prefecture University, Sakai-city, Osaka 599-8531, Japan.

‡ Deceased.

(1) Yang, P. L.; Schultz, P. G. *J. Mol. Biol.* **1999**, *294*, 1191−1201.
(2) Fox, T.; Scanlan, T. S.; Kollman, P. A. *J. Am. Chem. Soc.* **1997**, *119*, 11571−11577.
(3) Allen, D.; Cumano, A.; Simon, T.; Sablitzky, F.; Rajewsky, K. *Int. J. Cancer Suppl.* **1988**, *3*, 1−8.
(4) Ulrich, H. D.; Mundorff, E.; Santarsiero, B. D.; Driggers, E. M.; Stevens, R. C.; Schultz, P. G. *Nature* **1997**, *389*, 271−275.
(5) Mundorff, E. C.; Hanson, M. A.; Varvak, A.; Ulrich, H.; Schultz, P. G.; Stevens, R. C. *Biochemistry* **2000**, *39*, 627−632.
(6) Dewar, M. J. S.; Wade, L. E. J. *J. Am. Chem. Soc.* **1975**, *99*, 4417−4424.
(7) Baumann, H.; Chen, P. *Helv. Chim. Acta* **2001**, *84*, 124−140.
(8) Hrovat, D. A.; Beno, B. R.; Lange, H.; Yoo, H.-Y.; Houk, K. N.; Borden, W. T. *J. Am. Chem. Soc.* **1999**, *121*, 10529−10537.
(9) Haeffner, F.; Houk, K. N.; Reddy, Y. R.; Paquette, L. A. *J. Am. Chem. Soc.* **1999**, *121*, 11880−11884.
(10) Case, D. A.; Pearlman, D. A.; Caldwell, J. W.; Cheatham, T. E., III; Ross, W. S.; Simmerling, C.; Darden, T.; Merz, K. M.; Stanton, R. V.; Cheng, A.; Vincent, J. J.; Crowley, M.; Tsui, V.; Radmer, R.; Duan, Y.; Pitera, J.; Massova, I.; Seibel, G. L.; Singh, U. C.; Weiner, P.; Kollman, P. A. *Amber 6*, 6th ed.; University of California at San Francisco: San Francisco, 1999.

al.[11] The MM-PB/SA method is widely applied[12−15] and can successfully reproduce experimental binding free energies. The advantage to the MM-PB/SA method is that the binding free energy can be estimated from single MD trajectories of the antibody−hapten complexes in which the same set of snapshots is used to calculate the free energies of the complexes, hapten, and antibody. During the affinity maturation, the germ line antibody undergoes some replacement of residues in the light and the heavy chains. It is difficult to estimate the free energy difference using the widely used free energy perturbation approaches such as the thermal integration method[16,17] because the modifications are too large to treat by these methods. Chong et al.[13] applied the MM-PB/SA approach to estimate the binding free energy in the antibody 48G7 and reproduced absolute experimental free energies reasonably well and calculated very good relative free energies between germ line and mature.

For our project, we first address the intrinsic reaction coordinate (IRC) of oxy-Cope reaction in the gas phase using an ab initio molecular orbital (MO) method. B3LYP/6-31G* is found to be a suitable level of approximation; thus, the reactant (REA) and the transition state (TS) structure optimized at this level are used to make additional force field parameters for MM-MD simulations. Next, we will show the results of MD simulations of AZ28−hapten complexes for both the germ line and the mature catalytic antibody. Here, we can successfully reproduce the negative correlation shown in the experimental measurement[5] by using the MM-PB/SA method. To determine which somatic mutations contribute to the higher catalytic rate, alanine[18−20] and glycine scanning approaches are used to generate mutants for the same trajectory as the wild-type antibody simulation. We conclude that both the structural difference between TSA and TS and the greater flexibility of the germ line antibody play a key role in the high catalytic rate of the germ line antibody.

Methods

Figure 1 shows the schematic representation of the oxy-Cope rearrangement in AZ28 antibody. Unfortunately, the structure of the TS cannot be obtained experimentally, because the TS structure is not a stable one. Therefore, we have used a flexible model instead of using the real TS. This model is close to the optimized TS structure calculated by an ab initio MO method and is forced to have no imaginary normal-mode frequencies along the IRC reaction coordinate as if it were a stable molecule. Several harmonic restraints for the atom pairs are used in addition to usual Amber99 force field parameters.[21] This method is similar with the flexible free energy perturbation simulations by Stanton et al.[22] In their work "pseudobond" and "pseudoangle" harmonic restraint were introduced to ensure proper active-site geometry throughout the simulation.

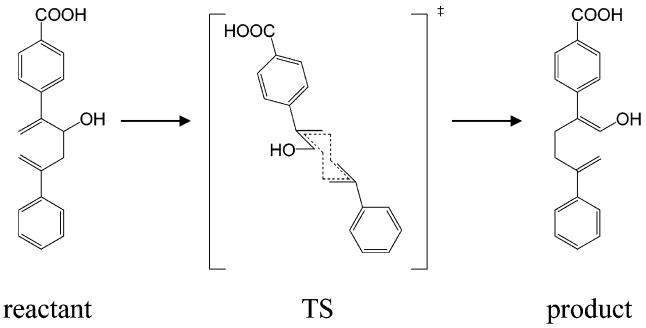

Figure 1. Schematic representation of the oxy-Cope rearrangement in the antibody AZ28.

Ab Initio MO calculations. We have calculated optimized structures for the neutral substrate (the reactant and the TS) by ab initio MO methods using the Gaussian 98 package[23] and determined the reaction path for the oxy-Cope rearrangement in the gas phase. Relative energies of the TS and the product based on REA structures have been calculated using different types of approximations and basis functions. We decided to use 6-31G* basis sets because Harold et al.[7] recently reported that B3LYP/6-31G* level of calculations are in good agreement with experimental results for oxy-Cope rearrangements. This is reasonable because all isolated structures of the substrate are neutral in charge, and the large basis set is not assumed to improve the quality of the calculation so much. The single-point energy calculations are also carried out using B3LYP/6-311++G** for the optimized structure obtained by B3LYP/6-31G*. In the ONIOM methods,[24,25] the central hexa-1,5-dien-3-ol moiety corresponding to the oxy-Cope rearrangement is treated quantum mechanically (HF/6-31G* and B3LYP/6-31G* level of approximations), and other atoms are calculated using the AM1 semiempirical level of approximations. To confirm the reliability of TS calculations, the HF and MP2 level of calculations are also applied to the similar 2,5-methyl-substituted hexa-1,5-dien-3-ol structures.

Model Structure Setting. X-ray crystal structures of the antibody AZ28[5] are used as starting structures for molecular dynamics simulations. The PDB ID codes are 1D6V with the resolution of 2.0 Å and 1AXS with the resolution of 2.6 Å for the germ line and the mature antibody AZ28−hapten complex, respectively. In the following discussions, we will sometimes denote the germ line and the mature forms of AZ28 as AZ28g and AZ28m, respectively. Substructures corresponding to F_v regions of the antibody have been extracted and used for MD simulations. All crystal water molecules are included in our calculations. Hydrogen atoms are added to heavy atoms of the crystal structure using the Leap module of the AMBER 6.0 package.[21] $His43^H$ and $His58^H$ (in the mature antibody) were protonated at the δ-nitrogen to make appropriate noncovalent bindings. As $His96^H$ is close to the binding site, both δ- and ϵ-protonation states were examined using the molecular mechanics interaction energy analysis. The hapten is treated

(11) Srinivasan, J.; Miller, J.; Kollman, P. A.; Case, D. A. *J. Biomol. Struct. Dyn.* **1998**, *16*, 671−682.
(12) Massova, I.; Kollman, P. A. *Perspect. Drug Discovery Des.* **2000**, *18*, 113−135.
(13) Chong, L. T.; Duan, Y.; Wang, L.; Massova, L.; Kollman, P. A. *Proc. Natl. Acad. Sci. U.S.A.* **1999**, *96*, 14330−14335.
(14) Kollman, P. A.; Massova, I.; Reyes, C.; Kuhn, B.; Huo, S.; Chong, L.; Lee, M.; Lee, T.; Duan, Y.; Wang, W.; Donini, O.; Cieplak, P.; Srinivasan, J.; Case, D. A.; Cheatham, T. E., III. *Acc. Chem. Res.* **2000**, *33*, 889−897.
(15) Lee, M. R.; Duan, Y.; Kollman, P. A. *Proteins: Struct., Funct., Genet.* **2000**, *39*, 309−316.
(16) Bash, P. A.; Singh, U. C.; Langridge, R.; Kollman, P. A. *Science* **1987**, *236*, 564−568.
(17) Allen, M. P.; Tildesley, D. J. *Computer Simulation of Liquids*; Clarendon Press: Oxford, 1987.
(18) Massova, I.; Kollman, P. A. *J. Am. Chem. Soc.* **1999**, *121*, 8133−8143.
(19) Dixon, R. W.; Kollman, P. *Proteins: Struct., Funct., Genet.* **1999**, *36*, 471−473.
(20) Kuhn, B.; Kollman, P. A. *J. Am. Chem. Soc.* **2000**, *122*, 3909−3916.
(21) Wang, J.; Cieplak, P.; Kollman, P. A. *J. Comput. Chem.* **2000**, *21*, 1049−1074.
(22) Stanton, R. V.; Perakyla, M.; Bakowies, D.; Kollman, P. A. *J. Am. Chem. Soc.* **1998**, *120*, 3448−3457.
(23) Frish, M. J.; Trucks, G. W.; Schlegel, H. B.; Gill, P. M. W.; Scuseria, G. E.; Robb, M. A.; Cheeseman, J. R.; Strain, M. C.; Burant, J. C.; Stratmann, R. E.; Dapprich, S.; Kudin, K. N.; Millan, J. M.; Daniel, A. D.; Petersson, G. A.; Montgomery, J. A.; Zakrzewski, V. G.; Raghavachari, K.; Ayala, P. Y.; Cui, Q.; Morokuma, K.; Foresman, J. B.; Cioslowski, J.; Ortiz, J. V.; Barone, V.; Stefanov, B. B.; Liu, G.; Liashenko, A.; Piskorz, P.; Chen, W.; Wong, M. W.; Andres, J. L.; Replogle, E. S.; Gomperts, R.; Martin, R. L.; Fox, D. J.; Keith, T.; Al-Laham, M. A.; Nanayakkara, A.; Challacombe, M.; Peng, C. Y.; Stewart, J. P.; Gonzales, C.; Head-Gordon, M.; Gill, P. M. W.; Johnson, B. G.; Pople, J. A. *Gaussian 98*; Gaussian: Pittsburgh, PA, 1998.
(24) Matsubara, T.; Maseras, F.; Koga, N.; Morokuma, K. *J. Phys. Chem.* **1996**, *100*, 2573−2580.
(25) Dapprich, S.; Komaromi, I.; Byun, K. S.; Morokuma, K.; Frisch, M. J. *J. Mol. Struct. (THEOCHEM)* **1999**, *461−462*, 1−21.

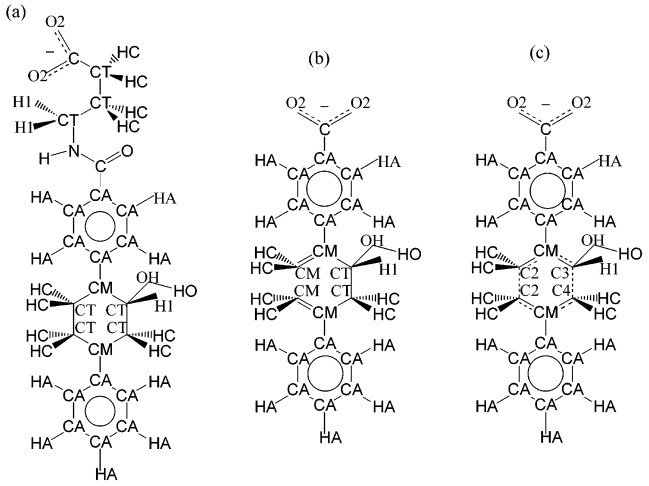

Figure 2. Atom types of Amber99 force field parameter sets used in our molecular dynamics simulations. In the transition-state structure three new atom types C2, C3, and C4 are introduced. (a) TSA. (b) Reactant. (c) Transition state.

as the anionic state in MD simulations because the carbonic acid group is likely to be deprotonated at neutral pH.

Starting structures for the REA and the TS are generated by superimposing to the TSA to minimize rmsd displacements. In this procedure, we restricted the position of the oxygen atom in the hydroxyl group of both REA and TS to be exactly the same as the corresponding oxygen atom in TSA. The atom types of TSA, REA, and TS are shown in Figure 2. Three new atom types, C2, C3, and C4 are introduced in the TS to reproduce ab initio optimized structures. The atomic partial charges of the hapten are calculated using RESP[26−28] software in the Amber 6.0 package, in which atomic charges are fitted to reproduce the electrostatic potential surrounding the molecule. Although there are various choices one can make to generate atomic charges, the RESP approach has some excellent features: (1) it is identical to the approach used to derive molecular mechanical electrostatic charges for the protein, thus automatically leading to balanced protein−protein and protein−substrate interactions, and (2) because the Lagrangian constraints can be employed in the RESP software, total charges of the substrate are restricted to be −1.0 *e* in our substrate. The detailed investigations of the RESP approach are carried out by Bayly et al.[26] The electrostatic potential are generated using HF/6-31G* and B3LYP/6-31G* for TSA and substrate, respectively. All RESP charges of substrates are shown in the Supporting Information: Figure 6 and Table 5. The bond, angle, dihedral parameters for the hapten not included in the AMBER99 force field parameters[21] are listed in Table 6 (in Supporting Information).

Molecular Dynamics Simulations. Molecular dynamics simulations are performed using the sander_classic module in the Amber 6.0 package. AZ28−hapten complexes are solvated by placing TIP3P cap water molecules within a radius of 42 Å from the geometrical center of the hapten. The geometry of each system is initially optimized with the steepest descent followed by the conjugate gradient energy minimization algorithms. The long-range nonbonded interaction is truncated using a 12 Å residue-based cutoff. However, some mutations can be observed up to 23 Å from the hapten. Therefore, we have also used a 25 Å secondary cutoff method, in which the energies and forces due to nonbonded interactions in the range from 12 to 25 Å are updated for every nonbonded pair list determination. In our simulations, only residues within 17 Å from the hapten geometrical center are allowed to move, and coordinates of the rest of the residues are frozen. The SHAKE algorithm is used to fix all bond lengths at equilibrium distances and to remove bond stretching, which is the fastest motion for all atomic displacements. The temperature of only the solvent molecules, including crystal water within 17 Å from the geometrical center of the hapten, which is called the belly region, are gradually heated from 0 to 300 K during the first 50 ps. Then, all residues within the belly region are equilibrated at 300 K for the next 500 ps with a time step of 2.0 fs, and following 500 ps trajectories are used to investigate the thermodynamic properties of the system. The temperature control is carried out using the Berendsen coupling scheme which uses separate scaling factors for atoms of the solute and the solvent to overcome the "cold solute/hot solvent" problem.[29]

Thermodynamic Properties. Binding free energies between AZ28 and the hapten are calculated using MM-PB/SA for 100 snapshots taken at 5-ps intervals from trajectories of each AZ28−hapten complex. In this method, the binding free energy ΔG_{bind} at each snapshot is approximated as

$$\Delta G_{bind} = \Delta E_{MM} + \Delta G_{solv} - T\Delta S \quad (1)$$

where, E_{MM} the molecular mechanics energy, G_{solv} the solvation free energy, T the absolute temperature, and S is the entropy of the solute.

As Massova[12] has pointed out, the relative contribution of the change in conformational entropy to ΔG_{bind} is negligible for the mutations. Thus, we also neglect the contribution of the last term in eq 1 in the following discussions because we are interested in the difference of ΔG_{bind} between the germ line and the mature antibody. The molecular mechanics energy E_{MM} is the sum of the binding E_{bind}, the angle E_{angle}, the dihedral E_{dihed}, the electrostatic E_{elec}, and van der Waals interactions E_{vdW}, which are determined by using the anal module. In the energy component analysis, no nonbonded cutoff is used.

The solvation free energy G_{solv} consists of the electrostatic contribution G_{PB} and the nonpolar contribution G_{np}.

$$G_{solv} = G_{PB} + G_{np} \quad (2)$$

where G_{PB} is calculated by solving the Poisson−Boltzmann (PB) equation. The Delphi 2.0 program[30] is used to solve the linearized differential PB equation. The atomic radii were taken from the PARSE parameter set[31] instead of using the Cornell et al. Force field[21,28] because of the small size of hydrogens. The same snapshots extracted from a single MD trajectory are used to calculate free energies of the complexes, the unbounded hapten, and the unbounded antibody for each AZ28−hapten complex. Because entropic effects of solvent molecules are effectively included in this G_{PB} term, all water molecules are removed from each trajectory before using the MM-PB/SA method. In the PB method, solvent molecules are treated as a continuous medium with the high relative dielectric constant ($\epsilon = 80$), and the solute is treated as low dielectric medium ($\epsilon = 1$). The solute dielectric of 1 is consistent with our use of a nonpolarizable molecular mechanics force field; in this model,[11−13,20,31] the solute response to charge fluctuations is estimated through explicit averaging of conformations, rather than by use of an interior dielectric greater than unity. The solvent dielectric of 80 is widely used for room-temperature water.[31] The nonpolar contribution term G_{np} is determined using the solvent accessible surface area (SASA) method by Sanner using the MSMS programs.[32]

$$G_{np} = \gamma(\text{SASA}) + \beta, \quad (3)$$

(26) Bayly, C. I.; Cieplak, P.; Cornell, W. D.; Kollman, P. A. *J. Phys. Chem.* **1993**, *97*, 10269−10280.
(27) Cornell, W. D.; Cieplak, P.; Bayly, C. I.; Kollman, P. A. *J. Am. Chem. Soc.* **1993**, *115*, 9620−9631.
(28) Cornell, W. D.; Cieplak, P.; Bayly, C. I.; Gould, I. R.; Merz, K. M. J.; Ferguson, D. M.; Spellmeyer, D. C.; Fox, T.; Caldwell, J. W.; Kollman, P. A. *J. Am. Chem. Soc.* **1995**, *117*, 5179−5197.
(29) Guenot, J.; Kollman, P. A. *J. Comput. Chem.* **1993**, *14*, 295−311.
(30) Nicholls, A.; Honig, B. *J. Comput. Chem.* **1991**, *12*, 435−445.
(31) Sitkoff, D.; Sharpe, K. A.; Honig, B. *J. Phys. Chem.* **1994**, *98*, 1978−1988.
(32) Sanner, M. F.; Olson, A. J.; Spehner, J.-C. *Biopolymers* **1996**, *38*, 305−320.

Table 1. Calculated Relative Energy for Substrate Based on the Reactant by ab Initio MO Method

method	relative energy (kcal/mol) TS	product
Substrate		
HF/STO-3G	42.2	−8.0
HF/6-31G*	50.3	−5.6
ONIOM (HF/6-31G*:AM1)	52.1	−4.3
ONIOM (MP2/6-31G*:AM1)	23.9	−4.5
B3LYP/6-31G*	23.2	−7.1
B3LYP/6-311++G**//B3LYP/6-31G*	25.1	−6.8
2,5-Methylhexa-1,5-dien-3-ol		
HF/6-31G*	54.9	−4.8
MP2/6-31G*	25.1	−5.5

where, γ and β are constant with the value of 0.00542 kcal/Å^2 and 0.92 kcal/mol, respectively. The probe radius to calculate SASA was 1.4 Å.[31]

Mutation Effects. During the maturation of AZ28g, two amino acid replacements in the light chain [Ser34^{L}Asn in the complementarily determining region L1 (CDRL1) and Ala51^{L}Thr in CDRL2] and four in the heavy chain [Tyr32^{H}Phe in CDRH1, Ser56^{H}Gly and Asn58^{H}His in CDRH2, and Thr73^{H}Lys in the framework region FR3] are observed.[5] To clarify these mutational effects on the binding free energies between the hapten and the antibody, the alanine scanning[18−20] techniques are applied. In the alanine scanning method, the C_γ atom of a given residue is replaced by a hydrogen atom which is located on the direction from C_β atom to C_γ atom at 0.94 Å far from C_β atom. In other words, the single trajectory obtained from the original MD simulation is used for residue mutations, and then MM-PB/SA calculations have been carried out for these mutated trajectories to calculate binding free energy for each mutant. The topology parameters have been changed appropriately to Ala. Similarly, the glycine scanning techniques are proposed in this work, because the alanine scanning method is not applicable when residues in one complex are originally Gly. In the glycine scanning method, C_β atom of a given residue is replaced with the hydrogen atom which is located on the direction from C_α atom to C_β atom at 0.94 Å far from C_α atom. The procedure to calculate free energy is same as the alanine scanning technique.

Results and Discussion

Structures and Energies of REA and TS. Table 1 shows the relative energies of TS and the product based on REA molecule using different types of approximations and basis functions. HF calculations predict high TS energy barriers in the oxy-Cope rearrangement which are larger than +42.2 kcal/mol. However, the delocalized bonding in the TS structure for the Cope rearrangement can be represented schematically as a resonance hybrid, containing contributions from two diradical extremes.[6,8] These resonance contributions should lower the activation enthalpy for the Cope rearrangement of 1,5-hexadien, as has been found to be the case experimentally by Doering et al.[33] Thus, we should consider electron correlation effects to calculate TS structures. Unfortunately, we could not optimize TS structure using a high level of approximations such as MP2/6-31G* because it requires large amount of storage and computational resources. Thus, first-layer ONIOM(MP2/6-31G*:AM1) approximations[25] are applied to include electron correlation effects for the central hexa-1,5-dien-3-ol part of molecule, in which the central hexa-1,5-dien-3-ol moiety is treated quantum mechanically and other atoms are calculated

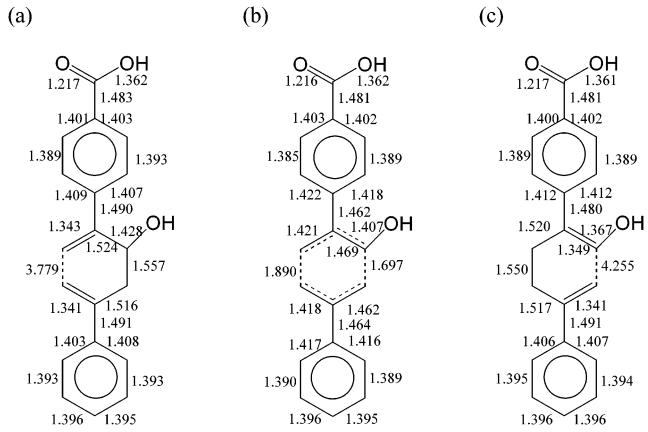

Figure 3. Optimized structures of substrates using B3LYP/6-31G* level of theory. Bond lengths are shown in the unit of Å. (a) Reactant. (b) Transition state. (c) Product.

using AM1 semiempirical level of theory. The ONIOM approximation increases the energy barrier high to +52.1 kcal/mol for the ONIOM (HF/6-31G*:AM1) calculation. However, the ONIOM (MP2/6-31G*:AM1) calculation successfully lowers the TS activation barrier to +23.9 kcal/mol, which is almost half of HF calculations. Additionally, we have used small-molecule models substituted by methyl groups at the 2- and 5-positions of the central hexa-1,5-dien-3-ol part of TSA structure; 2,5-methyl hexa-1,5-dien-3-ol. Interestingly, HF/6-31G* calculations for 2,5-methyl hexa-1,5-dien-3-ol roughly reproduce the order of the activation barrier of HF/6-31G* and ONIOM(HF/6-31G*:AM1) calculations of substrate. The MP2/6-31G* calculation of the 2,5-methyl hexa-1,5-dien-3-ol also shows approximately one-half of the barrier of the HF/6-31G* level of calculation. From these results we have concluded that electron correlation effects cannot be ignored for the oxy-Cope rearrangement. On the other hand, the density functional calculation of B3LYP/6-31G* allows us to optimize the whole molecule and shows a low barrier height of +23.2 kcal/mol which is close to MP2 level of theory. Thus, B3LYP/6-31G* can be considered as a reasonable approximation to investigate the oxy-Cope rearrangement as other authors have already pointed out.[7,8] Whereas the B3LYP/6-31G* calculation estimates the relative energy of the product to be small as −7.1kcal/mol, it is not important in this study because we have only used the free energy barrier between REA and TS structures. In addition, we have calculated the energy barrier using B3LYP/6-311++G**//B3LYP/6-31G*. Relative energies become +25.1 kcal/mol and −6.8 kcal/mol for TS and the product molecule, respectively.

According to the energy examinations above, structures and energies obtained from B3LYP/6-31G* calculations are reasonable to use in our simulations and discussions. The calculated bond lengths of optimized structures are shown in Figure 3. Whereas bond lengths in the central hexa-1,5-dien-3-ol substructure are dominantly changed during the oxy-Cope rearrangement, the rest of atoms such as substituted phenyl groups are maintained. Thus, we have created new atom types, C2, C3, and C4 for the central hexa-1,5-dien-3-ol part of TS structure (see Figure 2c), and normal atom types are used for stable parts of molecule to ensure proper active-site geometries throughout the simulation. We have used optimized bond lengths, angles,

(33) Doering, W. v. E.; Toscano, V. G.; Beasley, G. H. *Tetrahedron* **1971**, *27*, 5299.

Table 2. Comparison of Molecular Mechanics Interaction Energies between δ- and ϵ-Protonations of AZ28−Hapten (TS and TSA) Complexes in the Unit of kcal/mol

	germ line	mature
	TSA	
δ-protonation	−69.5	−72.2
ϵ-protonation	−64.6	−68.8
	TS	
δ-protonation	−74.4	−74.5
ϵ-protonation	−53.0	−55.7

dihedral angles to construct additional MM force field parameters for REA and TS, which are listed in Table 6.

In this system, it is well-known that the low activation barrier of oxy-Cope reaction originates from the high resonance of the TS.[8] Therefore, the two 2,5-phenyl groups in TS become parallel with respect to the central ring and look rather planar in contrast with the perpendicular structure in TSA.

Comparison of the Protonation of His96^H. The protonation of His96^H is important for hapten−antibody interactions because of directly hydrogen bonding with the hapten. Interaction energy analysis between the hapten and the antibody has been carried out for optimized structures of the germ line and the mature forms using the anal program. Table 2 shows calculated MM interaction energies. The δ-protonation His96^H of AZ28−TSA complex is more stable than the ϵ-protonation, with differences of stabilization energies of −4.9 and −3.4 kcal/mol for AZ28g and AZ28m, respectively. Also the differences in AZ28−TS complexes are −21.4 and −18.8 kcal/mol for AZ28g and AZ28m, respectively. Thus, it is most likely that His96^H has the δ-protonation. We have used the δ-protonation for His96^H residue in our MD simulations.

MD Simulation Results. MD simulations with explicit TIP3P water molecules at 300 K are carried out using the belly option. Figure 4 shows root-mean-square (rms) fluctuations of all atoms in the belly region from optimized structures for AZ28−TSA, AZ28−REA, and AZ28−TS complexes. We have obtained reasonably stable trajectories for all three complexes, in which rms fluctuations are from 1.0 to 1.5 Å. The fluctuations of AZ28g−TS complex are larger than other complexes. The comparison of these results shows that fluctuations of the germ line depend on the hapten (i.e., 1.2, 1.3, and 1.5 Å for REA, TSA, and TS, respectively) while the fluctuations of the mature complexes are almost same (ca. 1.0 Å) for all complexes. As expected, rms fluctuations of germ line complexes are always larger than mature configurations. The greater flexibility might arise because the germ line antibody must readily adapt to a variety of antigens. These features are also seen in the MD simulations for antibody 48G7−hapten complexes previously reported by Chong et al.[13]

The conformations of the active site in the MD structure averaged over the simulated time period 995−1000 ps are given in Figure 5. The long tail of the transition state analogue makes ionic bonds to Arg50^L by strong electrostatic interactions. The mature form makes two bonds in contrast with the germ line antibody with one bond as shown in Figure 5A,B. The oxygen atom in the hydroxyl group in TSA is bounded with His96^H, and AZ28m−TSA makes a second hydrogen bond with Glu35^H. On the other hand, the TS−antibody complexes have quite different conformations from the TSA−antibody complexes as shown in Figure 5C,D. The TS does not make favorable ionic

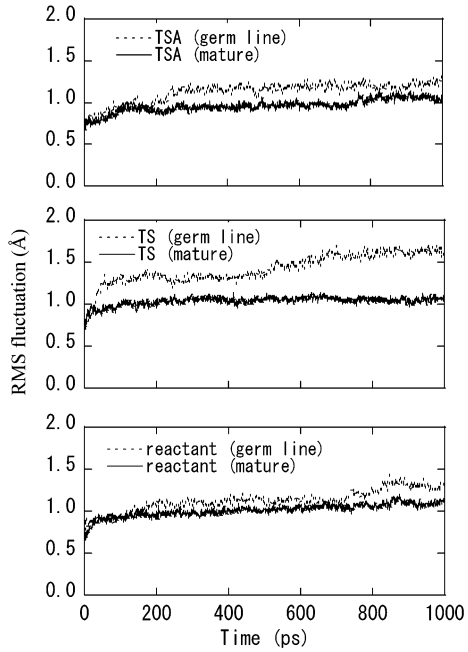

Figure 4. rms fluctuations calculated by MD simulations for the germ line and the mature antibody with TSA, TS, and REA. rms fluctuations are calculated to all atoms inside the belly region at a given time from each minimum energy conformation.

bonds with Arg50^L because it does not have the long tail of the TSA and the terminal carbonyl group of TS is exposed to liquid water. Thus, only one hydrogen bond can be seen in Figure 5C,D, in which the hydroxyl group in TS connects to Gly95^H for the germ line and to Asp101^H for the mature antibody.

The binding free energies are calculated using the MM-PB/SA approximation for AZ28−TSA, AZ28−TS, and AZ28−REA complexes (Table 3). The energetic analysis was done for only a single MD trajectory of the desired antibody−hapten complex with unbound antibody and hapten snapshots taken from snapshots of that trajectory. Therefore, the intramolecular energy contributions of the bonding, the angle and the dihedral angle terms to binding free energies exactly cancel out between the complex and the sum of the isolated hapten and the antibody.

First, we will discuss the difference of each energy component between the germ line and the mature forms. ΔE_{mm} is the molecular mechanics interaction energy consists of the electrostatic and van der Waals interactions, which has large contribution to the binding free energy with its large standard deviation. This large standard deviation mainly comes from the fluctuation of the electrostatic interaction ΔE_{elec}. ΔE_{mm} suggests that AZ28m is a more favorable antibody than AZ28g for TSA, in which the difference of molecular mechanics interaction energies is 33.0 kcal/mol. ΔG_{np} shows almost the same contribution to the binding free energy for all compounds because the structures are similar to each other although the tail differs between TS and TSA, but the effects are rather small. ΔG_{PB} also has large contribution to the binding free energy with its large standard deviations. The high dielectric constant for the solvent used in the PB method can roughly explain the reorientation of solvent water molecules which tend to eliminate large standard deviations of ΔE_{elec}. In this manner, the standard deviation of ΔG_{tot} considerably decreases taking the solvation free energy into consideration. ΔG_{tot} becomes −15.4 and −17.4 kcal/mol for AZ28g−TSA and AZ28m−TSA, respectively. The relative

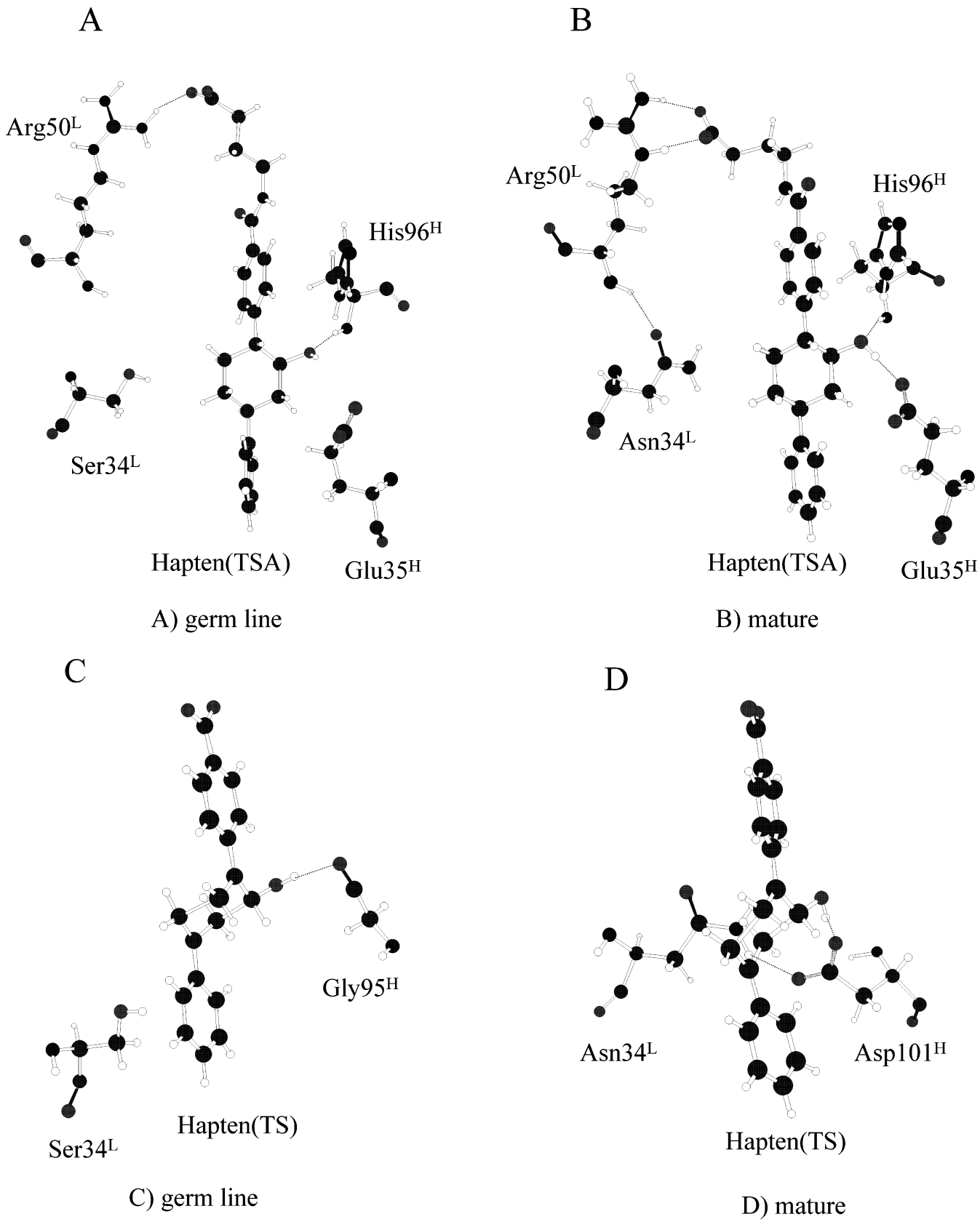

Figure 5. Conformations of active site with hydrogen bonding/ionic interactions between the hapten and the antibody in the MD simulation averaged over the simulated time period 995−1000 ps. The dashed lines give hydrogen bonding/ionic interactions. (A) AZ28g−TSA, (B) AZ28m−TSA, (C) AZ28g−TS, and (D) AZ28m−TS.

value of AZ28m−TSA based on AZ28g−TSA is −2.0 kcal/mol which is close to the experimental data of −2.1 kcal/mol, which means that the affinity for the hapten of AZ28m−TSA is greater than for AZ28g−TSA. The standard errors of ΔG_{tot}

Table 3. Energetic Analysis and Binding Free Energy Calculation of AZ28−Hapten Complex in kcal/mol[a]

TSA	germ line	mature	TS	germ line	mature	REA	germ line	mature
$\langle\Delta E_{elec}\rangle$	−26.4 (9.71)	−61.5 (12.6)	$\langle\Delta E_{elec}\rangle$	−19.6 (11.5)	11.5 (9.00)	$\langle\Delta E_{elec}\rangle$	−19.6 (12.5)	16.7 (8.83)
$\langle\Delta E_{vdw}\rangle$	−44.8 (2.91)	−42.7 (2.77)	$\langle\Delta E_{vdw}\rangle$	−29.2 (1.81)	−41.4 (1.90)	$\langle\Delta E_{vdw}\rangle$	−35.8 (2.75)	−41.1 (2.17)
$\langle\Delta E_{mm}\rangle$	−71.2	−104.2	$\langle\Delta E_{mm}\rangle$	−48.8	−29.9	$\langle\Delta E_{mm}\rangle$	−55.4	−24.4
ΔG_{np}	−5.3 (0.18)	−5.5 (0.09)	ΔG_{np}	−4.6 (0.27)	−4.8 (0.10)	ΔG_{np}	−5.0 (0.10)	−4.9 (0.10)
ΔG_{PB}	61.1 (10.4)	92.4 (11.8)	ΔG_{PB}	37.2 (12.8)	22.1 (9.10)	ΔG_{PB}	51.6 (10.5)	22.0 (10.7)
ΔG_{solv}	55.8	86.9	ΔG_{solv}	32.6	17.3	ΔG_{solv}	46.6	17.1
$\Delta G_{elec,tot}$	34.7 (4.12)	30.8 (4.68)	$\Delta G_{elec,tot}$	17.6 (3.44)	33.6 (3.65)	$\Delta G_{elec,tot}$	32.0 (4.81)	38.7 (4.27)
ΔG_{tot}	−15.4 (3.72)	−17.4 (4.04)	ΔG_{tot}	−16.2 (2.82)	−12.5 (3.33)	ΔG_{tot}	−8.8 (3.52)	−7.3 (4.42)

[a] The value in the angle bracketssignifies the averaged molecular mechanics interaction energy between the antibody and the hapten. The parenthesis shows the standard deviation in the MD simulation.

are 0.37 and 0.40 kcal/mol for AZ28g−TSA and AZ28m−TSA, respectively. The favorable binding free energy of the mature form for the TSA dominantly comes from the favorable $\Delta G_{elec,tot}$ of −3.9 kcal/mol which overcomes the unfavorable ΔE_{vdW} of +2.1 kcal/mol. In contrast, the binding affinity of AZ28g−TS is more stable than that of AZ28m−TS complex, in which the calculated difference of AZ28m−TS based on AZ28g−TS is +3.7 kcal/mol. The standard errors of ΔG_{tot} are 0.28 and 0.33 kcal/mol for AZ28g−TSA and AZ28m−TSA, respectively. ΔE_{mm} in AZ28−TS complexes suggests that AZ28g is a favorable antibody for TS, which is a more planar structure than TSA as discussed above. The difference of molecular mechanics interaction energies is 18.9 kcal/mol. This suggests that the germ line is flexible enough to adopt a more planar TS structure with favorable interaction with TS. ΔG_{tot} for AZ28m−REA and AZ28g−REA complexes are −7.3 and −8.8 kcal/mol, respectively. This free energy difference of +1.5 kcal/mol is the smallest one for the three kinds of hapten.

Now, the activation free energy barrier G_{act} for the oxy-Cope rearrangement in the antibody complex can be discussed using both binding free energies ΔG_{tot} and the activation energy in the gas-phase reaction of the substrate calculated by ab initio MO methods. To calculate G_{act}, ΔE_{TS*} should be considered with $\Delta G_{tot}(TS) - \Delta G_{tot}(REA)$ to change the configuration of the substrate from REA to TS. Therefore, G_{act} during the oxy-Cope rearrangement[34] is calculated by eq 4

$$G_{act} = \Delta G_{tot}(TS) - \Delta G_{tot}(REA) + \Delta E^*_{TS} \qquad (4)$$

The activation barrier ΔE_{TS}* calculated by ab initio MO method is +23.2 kcal/mol in B3LYP/6-31G* level of theory; thus, G_{act} becomes +15.8 kcal/mol and +18.0 kcal/mol for the germ line and the mature complexes, respectively. The activation free energy for the oxy-Cope rearrangement in the germ line antibody is 2.2 kcal/mol more stable than in the mature complex, which coincides with the experimental data of 2.2kcal/mol.[5] Therefore, we can conclude that the catalytic rate of the oxy-Cope reaction in the germ line complex is larger than that in the mature complex, while the binding affinity of the mature form for TSA is higher than that of the germ line. These results reproduce the negative correlation in antibody AZ28-catalyzed oxy-Cope rearrangement.

Next, we discuss the difference of each component for energy analysis between AZ28−TSA and AZ28−TS. The intermolecular interactions between the antibody and the hapten are very different between AZ28−TSA and AZ28−TS, especially for the electrostatic interaction in the mature complex.

In the mature complex, ΔE_{elec} of AZ28m−TSA has −61.5 kcal/mol despite +11.5 kcal/mol for AZ28m−TS. The positive electrostatic interaction of +16.7 kcal/mol is also observed in the AZ28m−REA complex. However, total electrostatic contributions of $\Delta G_{elec,tot}$ considering the ΔG_{PB} become +30.8 and +33.6 kcal/mol for AZ28m−TSA and AZ28m−TS, respectively, which are close to each other, because electrostatic interactions respond to ΔG_{PB} which tends to screen large electrostatic interactions. The ΔG_{tot} becomes −17.4 kcal/mol for AZ28m−TSA and −12.5 kcal/mol for AZ28m−TS, and the difference of −4.9 kcal/mol comes from the electrostatic contribution $\Delta G_{elec,tot}$ of −2.8 kcal/mol and from the nonpolar contribution of −2.1 kcal/mol.

In the germ line complex, all ΔE_{elec}'s have negative values forming favorable interactions between the antibody and the hapten. $\Delta G_{elec,tot}$ of AZ28g−TS is more stable than that for AZ28g−TSA, but ΔE_{vdW} for AZ28g−TS is unstable when comparing with that for AZ28g−TSA. Thus, ΔG_{tot}'s become −15.4 and −16.2 kcal/mol for AZ28g−TSA and AZ28g−TS, respectively. The difference is only +0.8 kcal/mol. These results show that the important features for the negative correlation between the affinity of AZ28−TSA and the catalytic rate of AZ28−substrate complexes dominantly comes from the large differential interactions of AZ28m−hapten complexes. The mature antibody has a favorable conformation to interact with TSA, but it is not flexible enough to accept the flat TS structure. In contrast, the germ line with high flexibility is deformable to adopt TS. Thus, we can conclude that the high catalytic rate of the oxy-Cope rearrangement in the germ line antibody comes from the favorable interaction between the TS and the germ line antibody.

Energy Analysis of Mutants Using Alanine and Glycine Scanning Methods. Using the MD trajectories obtained above, we have carried out the alanine and the glycine scanning approach to analyze mutation effects on the binding free energy between the antibody and the hapten. This approach replaces the specified residue in the amino acid sequences with either alanine or glycine while preserving respective conformations in each snapshot. Actually, the six somatic mutations during the maturation increase the affinity of the antibody for the hapten through interresidue interactions or conformational changes or both. However, the alanine/glycine scanning techniques used here cannot consider conformational changes. In this procedure, residues 34^L, 51^L, 32^H, 58^H, and 73^H are replaced to the alanine, and 56^H is replaced to the glycine in both the germ line and the mature forms.

Table 4 shows binding free energies ΔG for wild-type and mutants of AZ28m and AZ28g together with their component

(34) Kuhn, B.; Kollman, P. A. *J. Am. Chem. Soc.* **2000**, *122*, 2589−2596.

Table 4. Summary of Calculated Binding Free Energy in kcal/mol for Mutants of AZ28g and AZ28m Using the Alanine and the Glycine Scanning Methods

antibody	nonelectrostatic	electrostatic	$\Delta\Delta G_m$
AZ28g(TSA)	−50.1	34.7	0.0
AZ28m(TSA)	−48.2	30.8	0.0
AZ28g(TS)	−33.8	17.6	0.0
AZ28m(TS)	−46.2	33.6	0.0
AZ28g(TSA)Ser34^{L}Ala	−49.8	32.6	−1.8
AZ28g(TSA)Tyr32^{H}Ala	−50.0	34.7	0.1
AZ28g(TSA)Ser56^{H}Gly	−50.1	34.7	0.0
AZ28g(TSA)Asn58^{H}Ala	−50.1	34.6	−0.1
AZ28g(TSA)Thr73^{H}Ala	−50.1	34.7	0.0
AZ28m(TSA)Asn34^{L}Ala	−47.1	36.4	6.8
AZ28m(TSA)Thr51^{L}Ala	−48.2	30.8	0.0
AZ28m(TSA)Phe32^{H}Ala	−48.1	30.8	0.1
AZ28m(TSA)His58^{H}Ala	−48.2	30.8	−0.1
AZ28m(TSA)Lys73^{H}Ala	−48.2	30.9	0.1
AZ28g(TS)Ser34^{L}Ala	−33.3	16.8	−0.3
AZ28g(TS)Tyr32^{H}Ala	−33.7	17.7	0.2
AZ28g(TS)Ser56^{H}Ala	−33.8	17.6	0.0
AZ28g(TS)Asn58^{H}Ala	−33.8	17.7	0.0
AZ28g(TS)Thr73^{H}Ala	−33.8	17.6	0.0
AZ28m(TS)Asn34^{L}Ala	−45.2	40.3	7.6
AZ28m(TS)Thr51^{L}Ala	−46.2	33.7	0.0
AZ28m(TS)Phe32^{H}Ala	−46.1	33.7	0.2
AZ28m(TS)His58^{H}Ala	−46.2	33.6	0.0
AZ28m(TS)Lys73^{H}Ala	−46.2	33.7	0.1

analysis. All nonelectrostatic components have negative values, whereas electrostatic components have positive ones. $\Delta\Delta G_m$ refers to the relative stabilization free energies based on the corresponding wild-type AZ28m and AZ28g complexes, which indicate that the largest values are seen for the 34^{L} residue in mutants. The alanine scannings of 34^{L} residue stabilize the binding free energy of −1.8 kcal/mol for AZ28g (TSA) Ser34^{L}-Ala and −0.3 kcal/mol for AZ28g (TS) Ser34^{L}Ala, and destabilize +6.8 kcal/mol for AZ28m (TSA) Asn34^{L}Ala and +7.6 kcal/mol for AZ28m (TS) Asn34^{L}Ala complexes. The residue 34^{L} is located closest to the hapten (∼ 8 Å) for the six mutatable residues (see Figure 5), and the long side chain in the Asn34^{L} in the mature complex makes hydrogen bonds to the other atoms. The reason for the large difference of the binding free energy in mature complexes is the large change of the 34^{L} residue from Asn to Ala. The important point to note is that the difference of $\Delta\Delta G_m$ between wild-type AZ28m−hapten (TSA and TS) and the mutants of Asn34^{L}Ala is only 0.8 kcal/mol, which means that the mutation of the 34^{L} residue significantly affects the binding free energy of the mature complexes but does not change the relative binding free energy between TS and TSA complexes through the interresidue interaction. Thus, the interresidue interaction by this mutation has small effect on the negative correlation. However, the conformational changes, which are ignored in this study, could also play an important role in the negative correlation.

Conclusions

The negative correlation between the affinity for TSA and the catalytic rate of oxy-Cope rearrangement reaction for substrate in the antibody AZ-28 are investigated using ab initio MO methods and molecular mechanics MD simulations. The B3LYP/6-31G* level of calculations can reproduce a reasonable low activation barrier for the oxy-Cope rearrangement reaction in the gas phase, in which the activation energy is estimated to be about +23.2 kcal/mol. Ab initio MO calculations also predict that the TS structure has more planar conformation compared to that of TSA. From this structural difference the MD trajectory of AZ28−TS becomes very different from that of AZ28−TSA (see Figure 5). Although AZ28m can interact favorably with TSA compared with AZ28g, it becomes unfavorable with TS, because the rmsd fluctuation of AZ28m is lower than that of AZ28g, and the structure of AZ28m cannot change enough to make favorable interactions with TS. The favorable binding free energy of the mature form for TSA mainly comes from favorable total electrostatic binding free energy which overcomes the unfavorable binding vdW interactions.

The activation barriers for oxy-Cope rearrangements calculated by ab initio MO methods and the total binding free energy obtained by the MM-PB/SA method show that the catalytic rate of the oxy-Cope reaction in the germ line complex is larger than that in the mature complex, while the binding affinity of the mature form is higher than that of the germ line complex, which is known as the negative correlation. The important characteristic features for the negative correlation between the affinity of AZ28−TSA and the catalytic rate of AZ28−substrate complexes dominantly comes from large different interactions of AZ28m−hapten complexes. The low activation barrier of the oxy-Cope reaction originates from the high degree of resonance in the TS. We can conclude that the low flexibility in the mature complex cannot make a stable interaction with the hapten and that the relative total binding activation barrier becomes higher than that in the germ line complexes, leading to the negative rate correlation in the AZ28 antibody.

Finally, we have carried out the alanine and the glycine scanning approach to analyze mutation effects on the binding free energy between the antibody and the hapten. The mutation of 34^{L} residue significantly affects the binding free energy of the mature complexes through the interresidue interaction but does not change the relative binding free energy between TS and TSA complexes though the interresidue interaction. Thus, the interresidue interaction by this mutation has small effect on the negative correlation, but conformation changes due to the mutation could play the key role in the negative correlation.

Acknowledgment. T.A. gratefully acknowledges support from Ministry of Education, Culture, Sports, Science, and Technology in Japan. This work was supported by a National Institutes of Health (NIH) Grant GM-29079. I. D. Kuntz assisted in the preparation of this manuscript.

Supporting Information Available: Additional figure of atom names, the table of RESP charges, and force field parameters (PDF). This material is available free of charge via the Internet at http://pubs.acs.org.

JA020774A